IJE TRANSACTIONS A: Basics Vol. 26, No. 10, (October 2013) 1255-1266

International Journal of Engineering

Journal Homepage: www.ije.ir

# Optimization of Low Pressure Vortex Tube via Different Axial Angles of Injection Nozzles

N. Pourmahmoud, A. Jahangiramini*, A. Izadi

*Department of mechanical engineering, University of Urmia, Urmia, Iran*

*PAPER INFO*

*Paper history:*
Received 09 April 2013
Received in revised form 11 June 2013
Accepted 20 June 2013

*Keywords*:
Vortex Tube
Numerical Simulation
Axial Angle
Energy Separation
Total Pressure

*ABSTRACT*

In this article, a Ranque–Hilsch Vortex Tube has been optimized utilizing axial angles for nozzles. Effect of nozzles angles on the flow behavior has been investigated by computational fluid dynamics (CFD) techniques. A finite volume approach with the standard k–ε turbulence model has been used to carry out all the computations. The dimensions of the studied vortex tubes have been kept the same for all models and the performance of machine was studied under 5 different angles (β), namely 0, 2, 4, 6 and 8 degree adjusted to the nozzles. Achieving a minimum cold exit temperature is the main goal of this numerical research. The results show that utilizing this kind of nozzle improves the cooling capacity of device for most values of inlet mass flow rates. Finally, some results of the CFD models have been validated by the available experimental data which show reasonable agreement, and other ones are compared qualitatively.

**doi:** *10.5829/idosi.ije.2013.26.10a.15*

**NOMENCLATURE**

| | | | |
|---|---|---|---|
| C.O.R | Capacity of refrigeration | **Greek Symbols** | |
| D | Diameter of vortex tube [mm] | $\alpha$ | Cold mass fraction |
| k | Turbulence kinetic energy [$m^2/s^2$] | $\beta$ | Axial angle of nozzles |
| L | Length of vortex tube [mm] | $\varepsilon$ | Turbulence dissipation rate [$m^2/s^3$] |
| M.C.T | Minimum cold temperature | $\Delta T_c$ | Temperature difference between inlet and cold ends [K] |
| $\dot{m}c$ | Cold exit mass flow rate [g/s] | $\Delta T_h$ | Temperature difference between hot end and inlet [K] |
| $\dot{m}_{in}$ | Inlet mass flow rate [g/s] | $\rho$ | Density [kg/ $m^3$] |
| r | Radial distance measured from the centerline of tube [mm] | $\mu$ | Dynamic viscosity [kg /m.s] |
| R | Radius vortex tube | $\mu_t$ | Turbulent viscosity [ kg /m.s ] |
| T | Temperature [K] | $\tau_{ij}$ | Stress tensor components |
| z | Axial length from nozzle cross section [mm] | $\xi$ | Gradient of cold flow's total pressure along the center line of tube |

## 1. INTRODUCTION

Re-distribution of the total energy of inlet flow without any external work or heat is named Energy separation phenomenon, and it is merely a fluid dynamical process as it takes place in a device with no moving parts. In this way; the high pressure gas enters the vortex chamber tangentially through one or more nozzles and splits into two low pressure flows whose temperatures are higher and lower than the inlet flow. Separated cold or hot streams, can be employed according to the industrial requirements. However, the noticeable function of a vortex tube is almost spot cooling process. The vortex tube was invented in 1933 by French physicist George J. Ranque while conducting a research

*Corresponding Author Email: ajahangiramini@yahoo.com (A. Jahangiramini)

over vortex tube in the field of dust separation. He noticed the emitting of hot air from one side and cold air from the other.

Physicist Rudolf Hilsch, a German researcher, studied his findings and performed experimental and theoretical works on the flow inside the vortex tube to improve its efficiency. He explained that temperature separation occurs because of radial gradient of tangential velocity, resulting in frictional coupling between different layers of rotating flow, which leads to energy transfer from inner layers to outer layers via shear work [1, 2].

A vortex tube and energy separation mechanism is schematically displayed in Figure 1. In recent years, the techniques of computational fluid dynamics (CFD) modeling have been developed for further survey and clarification. Several theories have been presented for the reasons of formation of two vortex flows inside the vortex tube, of which two of them are more acceptable. According to the first theory, energy transfers from the inner layers to the outer layers via the shear work, due to radial gradient of the tangential velocity results in friction coupling between different layers. The second theory explains this phenomenon thermodynamically, and states that a free expansion inside the vortex tube is the reason for the formation of two vortex flows inside the tube. From the thermo dynamical point of view, it is impossible that a flow be separated into two parts, one with higher energy and the other with lower energy compared to that of the main flow in a constant pressure process .Thus, a concept may explain this phenomenon that flow should expand adiabatically at the end of the tube away from the nozzles from high pressure to low pressure [3].

Recent efforts have successfully utilized CFD modeling to explain the fundamental principles behind the energy separation produced by the vortex tube. Aljuwayhel et al. [4] utilized a fluid dynamics model of the vortex tube to understand the process that drives the temperature separation phenomena. Skye et al. [5] used a model similar to that of Aljuwayhel et al. [4]. Promvonge [6] applied an algebraic Reynolds stress model (ASM) for the simulation of a strongly swirling flow in a vortex tube and found that the use of ASM results in more accurate prediction than the k–ε model.

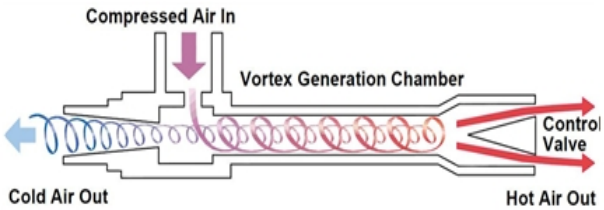


**Figure 1.** Schematic drawing of a vortex tube operational mechanisms.

Behera et al. investigated the effect of the different types and number of nozzles on temperature separation in a counter-flow vortex tube through CFD and experiment [7]. Their modeling of the vortex tube was carried out using the code system, Star-CD with 'Renormalization Group' (RNG) version of the k–ε model. Pourmahmoud et al. employed a full 3D numerical simulation to study the effect of helical nozzles on the energy separation in the vortex tube and proposed an appropriate profile for this kind of nozzles by introducing a new dimensionless number, i.e. GPL number [8, 9]. Subsequently, Pourmahmoud et al. investigated the importance of the lateral outflow effect of injection nozzles on the performance of vortex tube by numerous numerical simulations [10].

During 1960s, Takahama carried out experimental studies on pressure and temperatures inside the vortex tube and studied the effect of various geometric factors on its energy separation characteristics [11]. In 1977, Marshall [12] confirmed experimentally that separation is primarily dependent upon centrifugation. His results in comparing the Standard and the large tubes appear to indicate that the gas separation performance is the same if the effect of overall pressure drop is considered. Saidi and Valipour performed an experimental investigation to realize the behavior of a vortex tube system [13]. They investigated the effect of geometrical parameters, including diameter and length of the main tube, diameter of the outlet orifice, shape of the entrance nozzle and thermo-physical parameters such as inlet gas pressure, type of gas, cold gas mass ratio and moisture content of inlet gas. To study the effect of type of inlet nozzles, they designed and fabricated two shapes of nozzle having 3 and 4 intakes with constant inlet cross-sectional area. Their results showed that the nozzle with three intakes has better performance compared to the four intakes nozzle from the point of view of refrigeration efficiency. In 1997, Ahlborn and Groves [14] used a pitot tube to observe a secondary flow within the vortex tube. They concluded that the vortex tube must have a secondary circulation imbedded into the primary vortex, which moves the fluid from the back flow core to the outer regions.

Aydin and Baki experimentally studied the design parameters of a vortex tube, including the length of the vortex tube, three different diameters of 5, 6 and 7 mm for inlet nozzles and the angle of the control valve for three different working gases: air, oxygen and nitrogen. In their experiment showed that d = 6 mm was the optimum value of nozzle diameter and gave a higher total temperature difference [3].

Dincer et al. modeled the effects of length to diameter ratio and nozzle number on the performance of vortex tubes using artificial neural networks [15]. They examined 1, 2, 4, 6 and 8 inlet nozzles and concluded that the performance of vortex tube with 4, 6, 8 nozzles was better when compared with those with 1 and 2

nozzles. Kirmaci and Uluer also studied key design parameters of vortex tube [16]. Among those parameters five different orifices, each with two, three, four, five and six nozzles, were manufactured and used during the test. They concluded that the hot outlet temperature values changing from maximum to minimum have been obtained for the nozzle numbers of 2, 3, 4, 5, and 6, while the cold outlet temperature values varying from minimum to maximum have been obtained for the nozzle numbers of 3, 2, 4, 5, and 6, respectively. Shamsoddini and Hussein Nezhad numerically analyzed the effects of nozzle numbers on the flow and cooling power of a vortex tube [2]. They showed that as the number of the nozzles increases, the cooling power increases significantly while cold outlet temperature decreases moderately. Chang et al. [17] worked on different parameters of the divergence angle of hot tube, length of divergent hot tube and number of nozzle intakes. They showed that increasing number of nozzle intakes increases the sensitivity of temperature reduction and can obtain the highest possible temperature reduction. Valipour and Niazi examined the influence of uniform curvature of main tube on the performance of vortex tube in the terms of maximum temperature difference, the maximum refrigeration capacity and their Non-dimensional values [18]. Wu Y. T. et al [19] designed a new nozzle with equal gradient of Mach number. The designed device was equipped by a new intake flow passage for nozzles with equal flow velocity and was developed to reduce the flow energy loss. Dincer et al. [20] investigated experimentally for the best performance of machine with an emphasis on a plug located at the hot outlet. Investigated parameters were based on plug location, its diameter (5, 6, 7, 8 mm), the corresponding tip angle (30°, 60°, 90°, 120°, 150°, and 180°), number of nozzles (2, 4, 6), and supply inlet pressure in the range of 200–420 kPa. According to their results, it can be seen that the most efficient condition (maximum ΔT) is obtained for a plug diameter of 5 mm, tip angle about 30° or 60°, by keeping of the plug at position L, and letting the compressed air enter into the vortex tube through 4 nozzles. Pinar et al. [21] used Taguchi method under different conditions of inlet pressure, nozzle number and fluid type. They inferred that optimum results, maximum temperature gradient between the hot and cold outlets are obtained when the nozzle number is two (minimum number of nozzles).

More design parameters such as tube length and its geometry, cold and hot exit area, number of nozzles and the nozzles types include straight or helical shape can govern on the flow field behavior in a vortex tube. This research believes that axial angle of inlet nozzle can be one of the important geometrical parameters in proper employing of these nozzle types. The axial angle of inlet nozzle is named β. Therefore, the purpose of this article is to attain a meaningful value of β, so that the machine would operate in the way that maximum cooling effect or maximum refrigeration capacity is provided.

## 2. MATHEMATICAL FORMULATION

The compressible turbulent and high rotating flow inside the vortex tube is assumed as three-dimensional, steady state and the standard k–ε turbulence model is employed. Bramo and Pourmahmoud showed that because of good agreement of their numerical results with the experimental data, the k–ε model can be selected to simulate the effect of turbulence throughout the vortex tube as a computational domain [22]. They examined other advanced turbulence models such as the Reynolds stress equations and RNG k–ε models and finally concluded that these models do not lead to a convergence numerical solution. Consequently, the governing equations are arranged by the conservation of mass, momentum and energy equations, which are given by:

$$\frac{\partial}{\partial t}(\rho)+\frac{\partial}{\partial x_j}(\rho\tilde{u}_j)=0 \tag{1}$$

$$\frac{\partial}{\partial t}(\rho u_i)+\frac{\partial}{\partial x_j}(\rho\tilde{u}_j u_i-\tau_{ij})=-\frac{\partial p}{\partial x_i} \tag{2}$$

$$\frac{\partial}{\partial x_j}\left[u_i\rho\left(h+\frac{1}{2}\tilde{u}_j\tilde{u}_j\right)\right]=\frac{\partial}{\partial x_j}\left[k_{eff}\frac{\partial T}{\partial x_j}+u_i(\tau_{ij})_{eff}\right] \quad \& \quad k_{eff}=K+\frac{c_p\mu_t}{Pr_t} \tag{3}$$

Since we assumed the working fluid is an ideal gas, then the compressibility effect must be imposed so that:

$$p=\rho RT \tag{4}$$

The turbulence kinetic energy (k) and the rate of dissipation (ε) are obtained from the following equations:

$$\frac{\partial}{\partial t}(\rho k)+\frac{\partial}{\partial x_i}(\rho k u_i)=\frac{\partial}{\partial x_j}\left[\left(\mu+\frac{\mu_t}{\sigma_k}\right)\frac{\partial k}{\partial x_j}\right]+G_k+G_b-\rho\varepsilon-Y_M \tag{5}$$

$$\frac{\partial}{\partial t}(\rho\varepsilon)+\frac{\partial}{\partial x_i}(\rho\varepsilon u_i)=\frac{\partial}{\partial x_j}\left[\left(\mu+\frac{\mu_t}{\sigma_k}\right)\frac{\partial\varepsilon}{\partial x_j}\right]+C_{1\varepsilon}\frac{\varepsilon}{k}(G_k+C_{3\varepsilon}G_b)-C_{2\varepsilon}\rho\frac{\varepsilon^2}{k} \tag{6}$$

In these equations, Gk, Gb, and YM represent the generation of turbulence kinetic energy due to the mean velocity gradients, the generation of turbulence kinetic energy due to buoyancy and the contribution of the fluctuating dilatation in compressible turbulence to the overall dissipation rate, respectively. $C_{1\varepsilon}$ and $C_{2\varepsilon}$ are constants. σk and σε are the turbulent Prandtl numbers for k and ε also. The turbulent (or eddy) viscosity, $\mu_t$, is computed as follows:

$$\mu_t=\rho C_\mu\frac{k^2}{\varepsilon} \tag{7}$$

where, $C_\mu$ is a constant. The model constants $C_{1\varepsilon}$, $C_{2\varepsilon}$,

$C_\mu$, σk and σε have the following default values: $C_{1\varepsilon}$ = 1.44, $C_{2\varepsilon}$ = 1.92, $C_\mu$ = 0.09, σk = 1.0, σε = 1.3. Finite volume method with a 3D structured mesh is applied to the mentioned governing equations which is one of the numerical approaches to describe complex flow patterns in the vortex tube. Inlet air is considered as a compressible working fluid, where its specific heat, thermal conductivity and dynamic viscosity are taken to be constant during the numerical analysis procedure. Second order upwind scheme is utilized to discretive convective terms, and SIMPLE algorithm is used to solve the momentum and energy equations simultaneously. Because of highly non-linear and coupling virtue of the governing equations, lower under-relaxation factors ranging from 0.1 to their default amount are taken for the pressure, density, body forces, momentum, k, ε, turbulent viscosity and energy components to ensure the stability and convergence of the iterative calculations.

## 3. PHYSICAL MODELING

The geometry of the model and present created CFD model is identical to the vortex tube used by Skye et al. [5]. An ExairTM 708 slpm vortex tube which is illustrated in Figure 2 was used by Skye et al. [5], and we use this model to collect all the experimental data which is mentioned in this article. The geometry of the tube is given in Table 1 and Figure 3. In this numerical research, all geometrical properties of the Skye et al. [5] model are kept constant and performance of instrument optimized under different axial angles of injection nozzles. The radius and length of the vortex tubes were fixed at 5.7 mm and 106 mm, respectively. Since the nozzle consists of 6 nozzle heads; the CFD model has been assumed to be a rotational periodic flow and only a sector of the flow domain with angle of 60° is utilized, this can help to reach data faster than full model. The 3D CFD model with refinement in mesh along with boundary regions is shown in Figure 4a. In addition, for studying the effect of axial angle of nozzle (β) as new parameter, 5 different angles is used for the inlet nozzles as shown in Figure 4b.

Boundary conditions for the models are determined based on the experimental measurements by Skye et al. [5]. The inlet is modeled as a mass flow inlet. The specified total mass flow rate and stagnation temperature are fixed to 8.34 g/s and 294.2 K, respectively. Performance of vortex tube can change with its inlet parameters, so we did not change these parameters. Pressure of the inlet mass varies from experimental pressure of 4.8 bar [5], in order to discuss the effect of the inlet pressure. The static pressure at the cold exit boundary was fixed at experimental measurements pressure of 0.15 bars.

**TABLE 1 .** Geometry summary of the vortex tube model

| Parameter | Value |
|---|---|
| Working tube length (L) (mm) | 106 |
| Nozzle height (H) (mm) | 0.97 |
| Nozzle width (W) (mm) | 1.41 |
| Nozzle total inlet area (An) ($mm^2$) | 8.2 |
| Cold exit diameter (dc) (mm) | 6.2 |
| Cold exit area ($mm^2$) | 30.3 |
| Hot exit diameter (dh) (mm) | 11 |
| Hot exit area ($mm^2$) | 95 |
| Working tube I.D (D) (cm) | 1.14 |

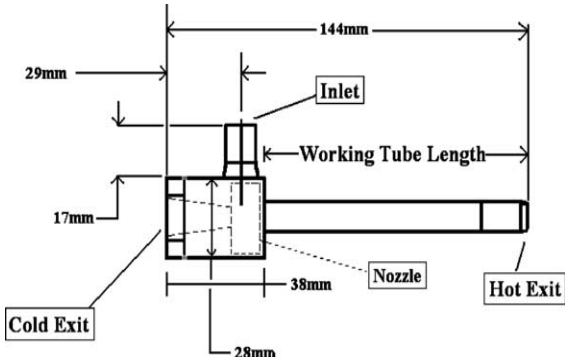


**Figure 2.** Schematic drawing of simulated an ExairTM 708 slpm model vortex tube.[6]

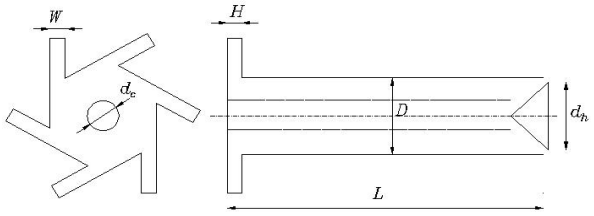


**Figure 3.** Illustration of the vortex tube geometry.

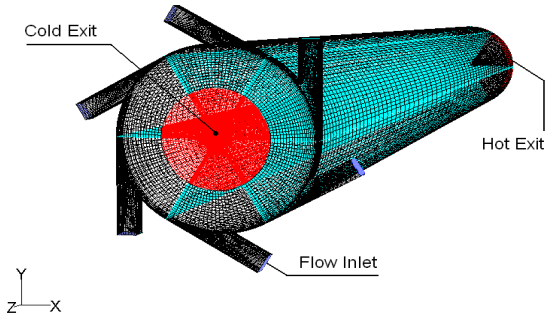


**Figure 4(a).** Three-dimensional CFD model of vortex tube with six straight nozzles

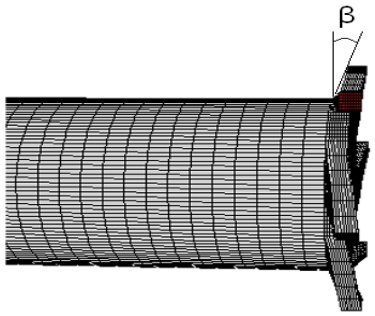


**Figure 4(b).** Definition of axial angle (β)

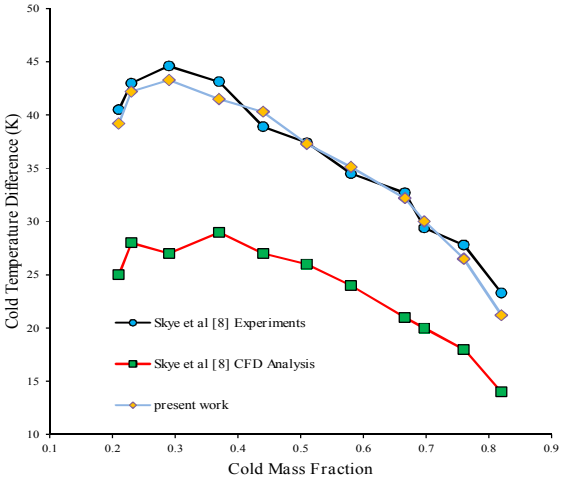


**Figure 5.** Comparison of cold exit temperature differences with the experimental data

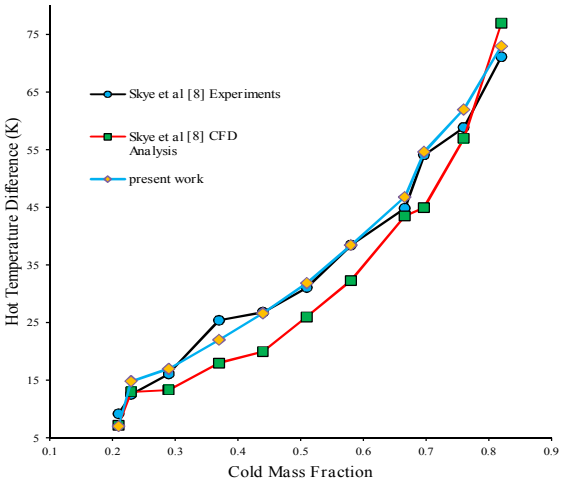


**Figure 6.** Comparison of hot exit temperature differences with the experimental data.

The static pressure at the hot exit boundary is adjusted in the way to vary the cold mass fraction. In addition, a no-slip velocity boundary condition is enforced on all of the walls of the vortex tube, and simultaneously they are assumed to be adiabatic.

In the CFD model, the hot exit was defined as a radial exit with a specified static pressure. The radial exit configuration is different from the axial exit associated with the experimental vortex tube; however, the flow distribution in the hot exit region has a negligible effect on the performance of a reasonably long vortex tube, and the CFD model was unable to converge when an axial exit was modeled [5].

## 4. VALIDATION

In the present computation, compressible forms of the Navier-Stokes equations and equation of state have been solved numerically by using the FLUENTTM software package together with appropriate k-ε turbulence model. The cold exit temperature difference ($\Delta T_c$) and the hot exit temperature difference ($\Delta T_h$) of the vortex tube are defined as following:

$$\Delta T_c = T_i - T_c \quad (8)$$

$$\Delta T_c = T_i - T_c \quad (9)$$

One of the important parameters which indicate the vortex tube performance and the energy separation in the vortex tube is cold mass fraction (α) that can be defined as the percentage of the air exiting through the cold end of the vortex tube to the pressurized air input and can be calculated by using Equation (10). The cold mass fraction can be controlled by the cone valve, which is placed at the hot end of the tube.

$$\alpha = \frac{\dot{m}_c}{\dot{m}_{in}} \quad (10)$$

where, $m_c$ is the mass flow rate at the inlet of the vortex tube and $m_{in}$ is outlet mass flow rate from cold end. The temperature difference obtained in the present analysis for the vortex tube with 6 straight nozzles is compared with the experimental and computational results of Skye et al in Figures 5 and 6. [5]. Both models use similar geometry and boundary conditions. The Skye et al. [5] CFD model was developed in a two-dimensional form, but the present one is three-dimensional, and this is an advantage of our modeling. $\Delta T_c$ is predicted to be somewhere between the experimental and computational results of Skye et al. [5]as shown in Figure 5. In Figure 6, the $\Delta T_h$, is predicted by proposed CFD model and is in good agreement with the corresponding experimental values.

The simulated $\Delta T_h$ at both models was close to the experimental results. Though, both models give $\Delta T_c$ lower than the experimental results, the prediction from the present model is found to be closer to the mentioned

experiment. In Figure 5, the maximum $\Delta T_c$ is obtained at a cold mass fraction (α) of about 0.3 through the experiment and CFD simulations. The applied 3D CFD model can produce hot gas temperature of 363.2 K at α = 0.8 and a minimum cold gas temperature of 250.24 K at about 0.3 cold mass fraction.

In the experiment, cold fractions can change directly with the pressure at the hot exit, and in CFD modeling, the static pressure at the hot exit boundary is adjusted in the way to vary the cold mass fraction. In addition, changing the hot exit pressure caused the cold exit pressure to change due to the pressure drop associated with the additional flow through the cold orifice as shown in Figure 7. The increase in the cold exit pressure results in a corresponding increase in the hot exit pressure. As seen in Figure 7, the model generally over-predicted the hot exit pressure required for a given cold fraction, however, the general trend agrees well. The model consistently over-predicted the hot exit pressure for data with cold fractions between 0.37 and 0.75. [5]

## 5. RESULTS AND DISCUSSIONS

**5. 1. Grid Independence Study** The 3D CFD analysis has been carried out for different average unit cell volumes in vortex tube as a computational domain. This is because of removing probable errors arising due to grid coarseness. Hence, first the grid independence study has been accomplished for α = 0.3. According to presented results in Figure 3, at this cold mass fraction the vortex tube (with 6 straight nozzles) attains a minimum outlet cold gas temperature. Thus, in the following evaluations we use α = 0.3 as a special value of cold mass fraction. The variation of cold exit temperature difference and maximum swirl (tangential) velocity as the key parameters are shown in Figures 8 and 9 respectively for different unit cell volumes. Not much significant advantage can be seen by reducing the unit cell volume size below 0.0257mm$^3$; which corresponds to 287,000 cells. The same type of unit cell volume of grids is used to study the introduced vortex tube with different skew nozzles.

**5. 2. Effect of Axial Angle of Nozzles** In vortex tube, shape type and number of inlet nozzles are important. So far, many investigations have been implemented on these parameters to achieve the best performance of vortex tube upon minimum cold outlet temperature. Skew nozzles are a new kind of nozzles shape which has not been investigated yet. To discuss the effect of these new shapes we decided to focus on different parameters such as maximum and minimum pressure, swirl velocity, cold exit and hot exit temperature and the effect of inlet pressure on cold and hot exit temperatures. In order to study the influence of skew nozzles, 5 different angles have been investigated for the vortex tube with fixed geometry. The angle of β describes the axial angle of inlet nozzles. Different amounts of β including 0°, 2°, 4°, 6° and 8° have been analyzed numerically.

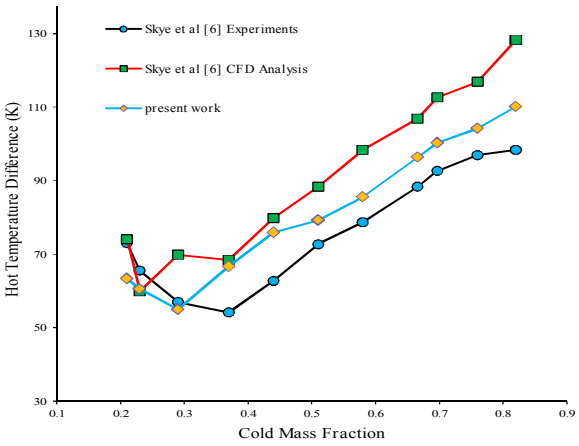


**Figure 7.** Experimentally measured and predicted hot and cold temperature separation as a function of cold fraction.

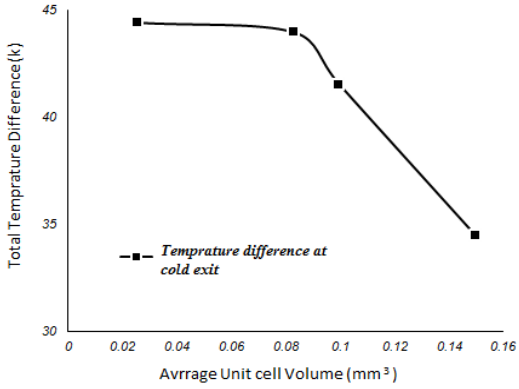


**Figure 8.** Grid size independence study on total temperature difference at different average unit cell volume.

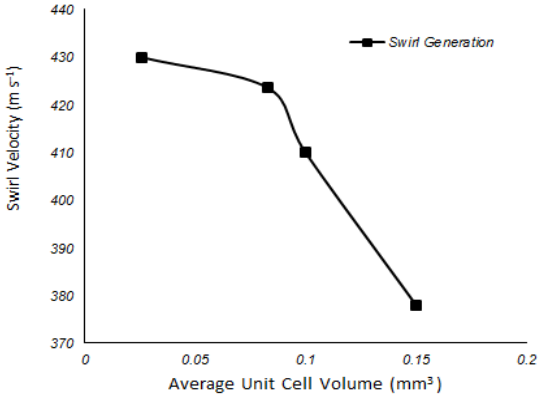


**Figure 9.** Grid size independence study on maximum swirl velocity at different average unit cell volume.

**5.2.1. Maximum and Minimum Pressure** Considering total pressure and static pressure of flow inside the tube, it can be understood that outer hot flow pressure, reduces along length of the tube towards its end, and for inner cold flow, it increases as shown in Figure 10. Results showed that the point where the maximum and minimum pressure occur and their values can be changed by using axial angles. These values would affect the behavior of fluid in the chamber of vortex tube. Table 2 represents the effect of axial angle variation on the maximum and minimum pressure for inlet pressure of 4.8 bars (Skye's et al. [5] operating pressure). The ξ parameter presents the gradient of cold flow's total pressure along center line of vortex tube in the corresponding maximum and minimum pressure points according to Equation (11).

$$\xi = \frac{\Delta P}{\Delta Z} = (P_{max} - P_{min})/(Z_{max} - Z_{min}) \quad (10)$$

According to the data of Table 2 the location of maximum pressure point becomes closer to the hot exit using the axial angle of nozzles and the values of minimum pressure increase. We believe that changing the parameter of ξ can directly affect the cold exit temperature. Because, when ξ is high, it means that cold flow pressure reduction is also high therefore the energy losses of flow becomes more and in this case the cold exit temperature decreases. So, it can be predicted that the cold exit temperature for $\beta = 0$ and $\xi = 0.555$ is lower than other models because it has the highest amount of ξ and the cold exit temperature for $\beta = 8°$ and $\xi = 0.514$ is higher than other models because it has the lowest amount of ξ. For other models, this theory is confirmed as well, i.e. the highest the ξ the highest $\Delta T_c$ and vice versa.

**5. 2. 2. Cold Exit and Hot Exit Temperature** As a critical parameter, temperature difference at cold exit and hot end of Tube is investigated under different inlet pressures and axial angles. Figures 11 and 12 show that using this kind of nozzles, the performance of instrument increases. So cold exit temperature would be lower utilizing β=4° in all cases except working pressure of Skye et al. [5]. Hot exit flow would be warmer for β=8°. It is noticeable that increasing the inlet pressure improves the efficiency of vortex tube.

Inlet pressure is changed from 3.47 to 4.8 bar and Figure 11 indicates that by increasing the inlet pressure from 3.47 to 4.8 bar (Skye's et al. [5] operating pressure), the cold exit temperature decreases. Figure 12 shows the changes of hot exit temperature with respect to applied inlet pressure. Since the rotating gas flow rate is encountered by the sheer stress of the layer and also friction caused by the tube wall; the overall behavior of the diagram has relatively increasing trends.

A vortex tube is used most often for cooling, not for heating. Hence, cold temperature is more important. It is evident that the inlet pressure should be increased, whatever much more cooling we want. It can be concluded that cold exit temperature would be lower utilizing β=4° for inlet pressures under Skye's working pressure and hot exit flow would be warmer for β=8° for all pressures.

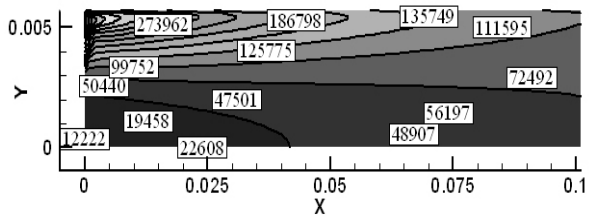


**Figure 10.** Contour of total pressure inside the tube

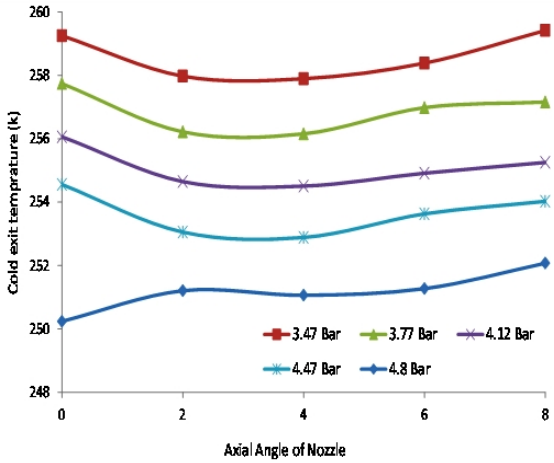


**Figure 11.** Cold exit temperature for various inlet pressures.

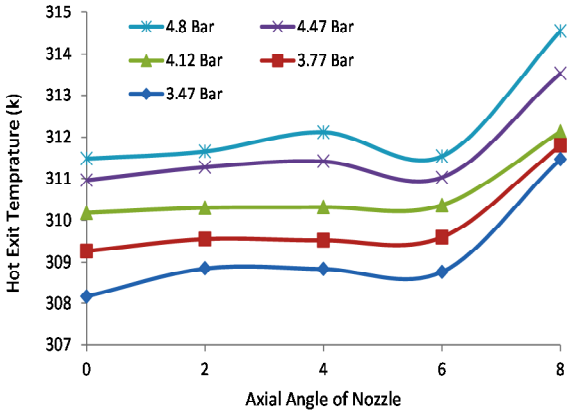


**Figure 12.** Hot exit temperature for various inlet pressures.

**TABLE 2.** Maximum and minimum pressure magnitudes along center line of vortex tube for cold flow

| β | Z min (mm) | Z max (mm) | P min (KPa) | P max (KPa) | Ξ |
|---|---|---|---|---|---|
| 0 | 6.76 | 102.7 | 10.48 | 63.69 | 0.555 |
| 2 | 5.97 | 103 | 11.24 | 62.45 | 0.528 |
| 4 | 5.97 | 103 | 11.38 | 62.93 | 0.531 |
| 6 | 5.97 | 103 | 11.49 | 62.46 | 0.525 |
| 8 | 5.97 | 103 | 11.91 | 61.75 | 0.514 |

**5. 2. 3. Swirl and Axial Velocity and Temperature Distributions** In order to realize the influence of nozzle type on the operating behavior of vortex tube, radial profiles of axial velocity and the swirl velocity at different axial locations have been shown in Figures 13-16 for β=0 and 4º. Analyzing the CFD models revealed that applying axial angle reduces the amount of swirl velocity respect to straight nozzles but the amount of this reduction is very low. Various dimensionless axial length such as z/L = 0.1, 0.4 and 0.7 are selected and the velocity profiles are analyzed for certain cold mass fraction of 0.3 at a location near the wall.

Results showed that the swirl velocity has the highest velocity component in comparison with the other ones. The radial distribution of swirl velocity profile in Figures 13 and 14 indicates a free vortex near the tube wall so that the values the values become negligibly small at the core of tube. Also, the same trend of axial and swirl velocity curves are reported by Behera et al. [7]. Finally as it is seen, increasing axial distance from inlet zone (z/L), towards the hot end causes the decrease of velocity components.

Swirl patterns of velocity magnitudes at the mid-plane of vortex chamber are shown in Figures 17-21 for different axial angles of injection nozzles. Indeed, vortex chamber is a place that, cold exit completely coincided to the end of plane, but with smaller diameter than the main tube. As illustrated in swirl patterns, utilizing axial angles of injection nozzles will increase velocity magnitude in the vortex chamber, and this means, efficiency of instrument will improve. The performance of a vortex chamber can be justified by two important facts of achieving the highest magnitude of swirl velocity and observing symmetrical flow field in the capability of energy injection to highly rotating flow. By increasing axial angle of injection nozzles, magnitude of swirl velocity can be increased, but symmetrical flow field would not be acceptable according to model with no angles. Considering both magnitude of swirl velocity and observing symmetrical flow field, injection nozzles with β=4° would have higher efficiency than other nozzles with axial angles. The total temperature distribution for vortex tube with β = 4° is displayed in Figure 22. Clearly, it can be seen that peripheral flow is warmer than the core flow. Furthermore, increase of temperature is observed in the radial direction. Under these operational and geometrical conditions, the machine provides the maximum hot and minimum cold gas temperatures of 312.12 K and 251.24 K respectively, when the cold mass fraction is about 0.3.

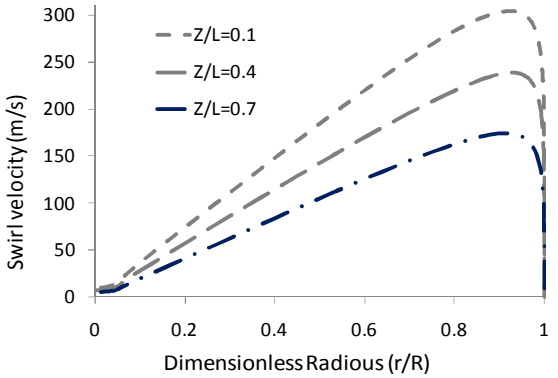


**Figure 13.** Radial profiles of the swirl velocity at different axial locations for β= 0º

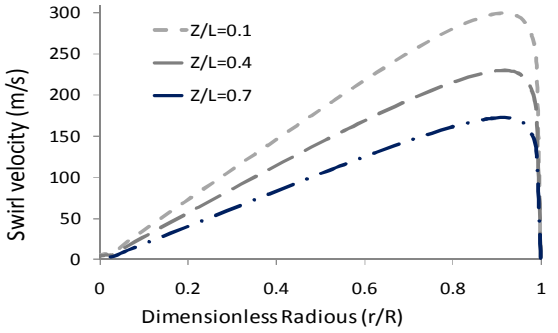


**Figure 14.** Radial profiles of the swirl velocity at different axial locations for β= 4º

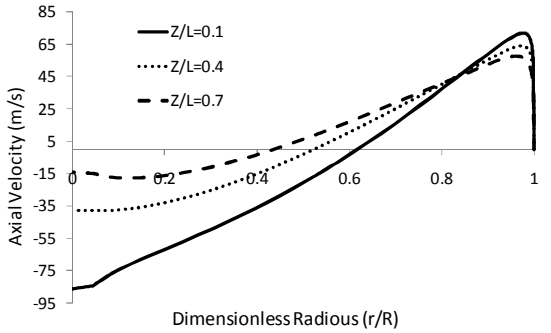


**Figure 15.** Radial profiles of the axial velocity at different axial locations for β= 0º

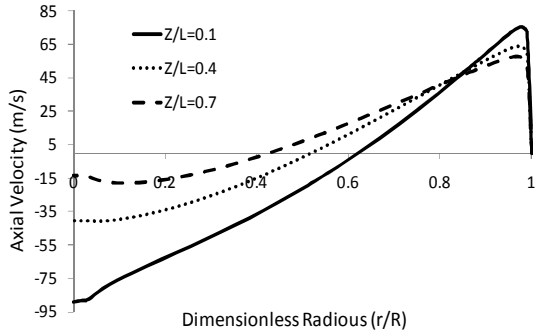


**Figure 16.** Radial profiles of the axial velocity at different axial locations for β= 4º

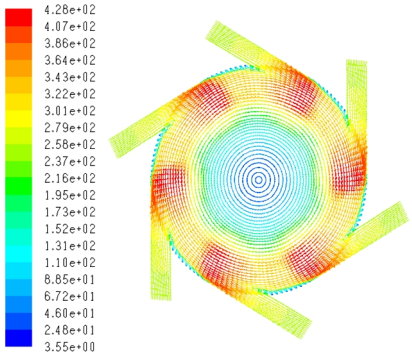


**Figure 17.** Swirl pattern at vortex chamber for β= 0º

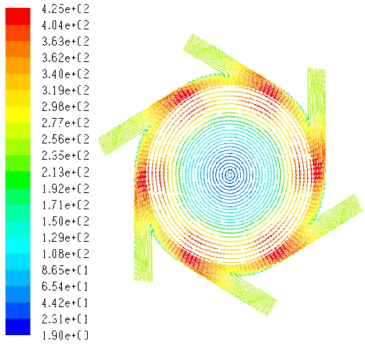

**Figure 18.** Swirl pattern at vortex chamber for β= 2º

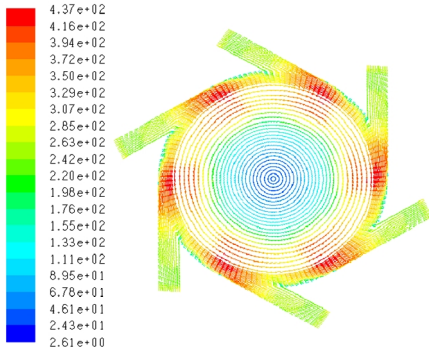


**Figure 19.** Swirl pattern at vortex chamber for β= 4º

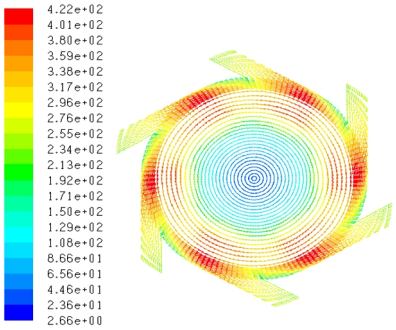


**Figure 20.** Swirl pattern at vortex chamber for β= 6º

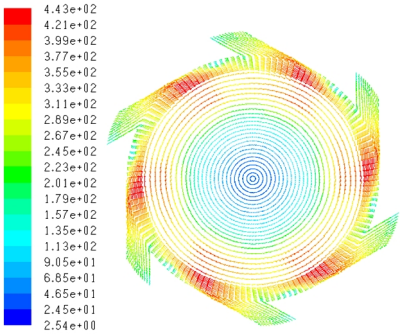


**Figure 21.** Swirl pattern at vortex chamber for β= 8º

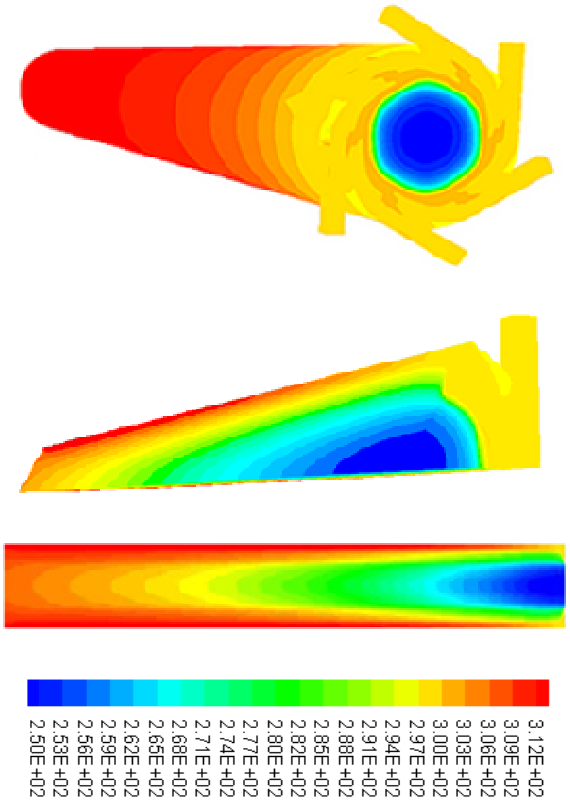


**Figure 22.** Temperature Distribution for β = 4.

## 6. CONCLUSION

A numerical analysis has been carried out to simulate a three dimensional, compressible, and turbulent fluid flow throughout a vortex tube. A symmetrical geometry and steady state flow has been assumed, and for exhibiting the turbulent flow structure inside vortex tube the standard k–ε turbulence model is employed. Simulations were conducted at 5 different angles of inlet nozzles. The effects of axial angle of nozzles and inlet pressure on the temperature separation were studied and lead to attain a reasonable and optimum axial angle for these kinds of nozzles. According to our results, the vortex tube with axial angle of $\beta = 4°$ operates the best condition from cooling point of view and axial angle with $\beta = 8°$ has maximum heating efficiency. Results showed that $\xi$ parameter has a direct relation with the energy separation phenomenon. The cold mass fraction was also varied by means of changing hot exit area. Comparison of present numerical results with measured experimental data, revealed a reasonable agreement data's predicted by employed CFD models were found to be in good agreement with each other. By considering new parameter $\xi$, predicting change of cold exit temperature is possible. According to our results, there is a relation between the pressure gradient along centerline of tube and cold exit temperature such that as the ratio of pressure gradient to distance difference is higher, the cold exit becomes lower.

## 7. REFERENCES


1. Hilsch, R., "Die expansion von gasen in zentrifugalfeld als kälteprozess", ***Zeitschrift Naturforschung Teil A***, Vol. 1, (1946), 208.
2. Shamsoddini, R. and Nezhad, A. H., "Numerical analysis of the effects of nozzles number on the flow and power of cooling of a vortex tube", ***International Journal of Refrigeration***, Vol. 33, No. 4, (2010), 774-782.
3. Aydın, O. and Baki, M., "An experimental study on the design parameters of a counterflow vortex tube", ***Energy***, Vol. 31, No. 14, (2006), 2763-2772.
4. Aljuwayhel, N., Nellis, G. and Klein, S., "Parametric and internal study of the vortex tube using a CFD model", ***International Journal of Refrigeration***, Vol. 28, No. 3, (2005), 442-450.
5. Skye, H., Nellis, G. and Klein, S., "Comparison of cfd analysis to empirical data in a commercial vortex tube", ***International Journal of Refrigeration***, Vol. 29, No. 1, (2006), 71-80.
6. Promvonge, P., "Numerical simulation of turbulent compressible vortex tube flow", Sanfrancisco, USA, ASME/JSME Joint Fluid Engineering, (1999).
7. Behera, U., Paul, P., Kasthurirengan, S., Karunanithi, R., Ram, S., Dinesh, K., and Jacob, S., "CFD analysis and experimental investigations towards optimizing the parameters of ranque–hilsch vortex tube", ***International Journal of Heat and Mass Transfer***, Vol. 48, No. 10, (2005), 1961-1973.
8. Pourmahmoud, N., Zadeh, H. A., Moutaby, O. and Bramo, A., "CFD analysis of helical nozzles effects on the energy separation in a vortex tube", ***Thermal Science***, Vol. 16, No. 1, (2012), 151-166.
9. Pourmahmoud, N., Hassanzadeh, A. and Moutaby, O., "Numerical analysis of the effect of helical nozzles gap on the cooling capacity of ranque–hilsch vortex tube", ***International Journal of Refrigeration***, Vol. 35, No. 5, (2012), 1473-1483.
10. Pourmahmoud, N., Izadi, A., Hassanzadeh, A. and Jahangiramini, A., "Computational fluid dynamics analysis of the influence of injection nozzle lateral outflow on the performance of ranque-hilsch vortex tube", ***Thermal Science***, (2013), 2-2.
11. Takahama, H., "Studies on vortex tubes:(1) experiments on efficiency of energy separation:(2) on profiles of velocity and temperature", ***Bulletin of JSME***, Vol. 8, No. 31, (1965), 433-440.
12. Marshall, J., "Effect of operating conditions, physical size and fluid characteristics on the gas separation performance of a linderstrom-lang vortex tube", ***International Journal of Heat and Mass Transfer***, Vol. 20, No. 3, (1977), 227-231.
13. Saidi, M. and Valipour, M., "Experimental modeling of vortex tube refrigerator", ***Applied Thermal Engineering***, Vol. 23, No. 15, (2003), 1971-1980.
14. Ahlborn, B. and Groves, S., "Secondary flow in a vortex tube", ***Fluid Dynamics Research***, Vol. 21, No. 2, (1997), 73-86.
15. Dincer, K., Tasdemir, S., Baskaya, S. and Uysal, B., "Modeling of the effects of length to diameter ratio and nozzle number on the performance of counterflow ranque–hilsch vortex tubes using artificial neural networks", ***Applied Thermal Engineering***, Vol. 28, No. 17, (2008), 2380-2390.
16. Kirmaci, V. and Uluer, O., "An experimental investigation of the cold mass fraction, nozzle number, and inlet pressure effects on performance of counter flow vortex tube", ***Journal of Heat Transfer***, Vol. 131, No. 8, (2009).
17. Chang, K., Li, Q., Zhou, G. and Li, Q., "Experimental investigation of vortex tube refrigerator with a divergent hot tube", ***International Journal of Refrigeration***, Vol. 34, No. 1, (2011), 322-327.
18. Valipour, M. S. and Niazi, N., "Experimental modeling of a curved ranque–hilsch vortex tube refrigerator", ***International Journal of Refrigeration***, Vol. 34, No. 4, (2011), 1109-1116.
19. Wu, Y., Ding, Y., Ji, Y., Ma, C. and Ge, M., "Modification and experimental research on vortex tube", ***International Journal of Refrigeration***, Vol. 30, No. 6, (2007), 1042-1049.
20. Dincer, K., Baskaya, S., Uysal, B. and Ucgul, I., "Experimental investigation of the performance of a ranque–hilsch vortex tube with regard to a plug located at the hot outlet", ***International Journal of Refrigeration***, Vol. 32, No. 1, (2009), 87-94.
21. Pinar, A. M., Uluer, O. and Kırmaci, V., "Optimization of counter flow ranque–hilsch vortex tube performance using taguchi method", ***International Journal of Refrigeration***, Vol. 32, No. 6, (2009), 1487-1494.
22. Bramo, A. R. and Pourmahmoud, N., "Computational fluid dynamics simulation of length to diameter ratio effects on the energy separation in a vortex tube", ***Thermal Science***, Vol. 15, No. 3, (2011), 833-848.

# Optimization of Low Pressure Vortex Tube via Different Axial Angles of Injection Nozzles

N. Pourmahmoud, A. Jahangiramini, A. Izadi

*Department of mechanical engineering, University of Urmia, Urmia, Iran*

*PAPER INFO*

*Paper history:*
Received 09 April 2013
Received in revised form 11 June 2013
Accepted 20 June 2013

*Keywords*:
Vortex Tube
Numerical Simulation
Axial Angle
Energy Separation
Total Pressure

**چکیده**

در این مقاله زاویه‌ی محوری نازل‌های تزریق دستگاه ورتکس تیوب رانک–هیلش بهینه سازی شده است. بررسی تأثیر زاویه‌ی نازل‌های تزریق بر رفتار جریان در ورتکس تیوب با استفاده از فنون دینامیک سیالات محاسباتی صورت گرفته و برای انجام تمام محاسبات از روش حجم محدود با مدل توربولانس استاندارد k-ε استفاده شده است. ابعاد ورتکس تیوب‌های مدل‌شده برای تمام مدل‌ها یکسان بوده و عملکرد دستگاه تحت ۵ زاویه‌ی محوری مختلف ۰، ۲، ٤، ٦ و ۸ درجه برای نازل‌ها بررسی شده است. رسیدن به حداقل دمای ممکن در خروجی سرد هدف اصلی این تحقیق عددی است. نتایج کار ما نشان می‌دهد که استفاده از این نوع نازل، ظرفیت سرمایشی دستگاه را برای اکثر نرخ‌های جریان جرمی بهبود می‌بخشد. در نهایت، برخی از نتایج حاصل از کار عددی با نتایج تجربی در دست مقایسه شده‌اند که تطابق قابل قبولی بین آنها وجود دارد.

**doi:** *10.5829/idosi.ije.2013.26.10a.15*